NOSC TD 1250

AD-A194 763

FILE COPY

NOSC

NAVAL OCEAN SYSTEMS CENTER San Diego, California 92152-5000

(4)

NOSC TD 1250

Technical Document 1250
April 1988

Metal Grid Base Heterojunction Transistor Operating at 60 and 94 GHz

H. Yamasaki, S. X. Bar
B. M. Paine, M. J. Tejwani

Hughes Aircraft Company

Sponsored by Defense Advanced
Research Projects Agency
ARPA Order No. 4766

Approved for public release; distribution is unlimited.

The views and conclusions contained in this report are those of the authors and should not be interpreted as representing the official policies, either expressed or implied, of the Naval Ocean Systems Center or the U.S. Government.

BEST
AVAILABLE COPY

UNCLASSIFIED

SECURITY CLASSIFICATION OF THIS PAGE

REPORT DOCUMENTATION PAGE

Field	Entry
1a. REPORT SECURITY CLASSIFICATION	UNCLASSIFIED
1b. RESTRICTIVE MARKINGS	
2a. SECURITY CLASSIFICATION AUTHORITY	
2b. DECLASSIFICATION/DOWNGRADING SCHEDULE	
3. DISTRIBUTION/AVAILABILITY OF REPORT	Approved for public release; distribution is unlimited.
4. PERFORMING ORGANIZATION REPORT NUMBER(S)	W-4A194
5. MONITORING ORGANIZATION REPORT NUMBER(S)	NOSC TD 1250
6a. NAME OF PERFORMING ORGANIZATION	Hughes Aircraft Company
6b. OFFICE SYMBOL (if applicable)	
7a. NAME OF MONITORING ORGANIZATION	Naval Ocean Systems Center
6c. ADDRESS (City, State and ZIP Code)	Microwave Products Division 3110 W. Lomita Blvd. Torrance, CA 90509-2940
7b. ADDRESS (City, State and ZIP Code)	Space Systems and Technology Division San Diego, CA 92152-5000
8a. NAME OF FUNDING/SPONSORING ORGANIZATION	Defense Advanced Research Projects Agency
8b. OFFICE SYMBOL (if applicable)	DARP-DSO
9. PROCUREMENT INSTRUMENT IDENTIFICATION NUMBER	N66001-86-C-0438
8c. ADDRESS (City, State and ZIP Code)	Defense Sciences Office 1400 Wilson Blvd. Arlington, VA 22209

10. SOURCE OF FUNDING NUMBERS

PROGRAM ELEMENT NO.	PROJECT NO.	TASK NO.	AGENCY ACCESSION NO.
61101E	DARP	760-EE66B	ICEE6 6B0

11. TITLE (include Security Classification)

METAL GRID BASE HETEROJUNCTION TRANSISTOR OPERATING AT 60 AND 94 GHz

12. PERSONAL AUTHOR(S)

H. Yamasaki, S.X. Bar, B.M. Paine, M.J. Tejwani

13a. TYPE OF REPORT	13b. TIME COVERED	14. DATE OF REPORT (Year, Month, Day)	15. PAGE COUNT
Interim Report #1	FROM Sep 1986 TO Sep 1987	April 1988	55

16. SUPPLEMENTARY NOTATION

17. COSATI CODES

FIELD	GROUP	SUB-GROUP

18. SUBJECT TERMS (Continue on reverse if necessary and identify by block number)

high frequency transistors; metal-organic chemical vapor deposition; lateral epitaxy; AlGaAs; heterojunctions; EHF; SIMS; X-Ray diffraction

19. ABSTRACT (Continue on reverse if necessary and identify by block number)

This program is for the development of a new device structure, the Metal Gridded Base Heterojunction Transistor (MGBHT). The device is an AlGaAs/GaAs bipolar structure, and incorporates a metal grid for reduction of the base resistance relative to a standard heterojunction transistor. In this reporting period, the device has been modeled analytically to verify performance potential and determine the required process parameters. Techniques for preparation of the metal grids have been developed, first with Ti-W, and later with pure W. Extensive experiments were conducted on epitaxial growth of GaAs and AlGaAs over the metal, and doping of GaAs and AlGaAs. Epitaxy is by metal-organic chemical vapor deposition, and Be and Zn have been used as the p-type dopants. A complete overhaul of the MOCVD reactor was completed in order to accommodate the Be dopant, as well as for incorporating very slow growth rates (50-100 Å/min). To date, Be doping has been achieved to levels of 2×10^{19} at/cm^3, with layer abruptnesses of about 100 Å.

Field	Entry
20. DISTRIBUTION/AVAILABILITY OF ABSTRACT	☐ UNCLASSIFIED/UNLIMITED ☒ SAME AS RPT ☐ DTIC USERS
21. ABSTRACT SECURITY CLASSIFICATION	UNCLASSIFIED
22a. NAME OF RESPONSIBLE INDIVIDUAL	J.R. Zeidler
22b. TELEPHONE (include Area Code)	(619) 553-1581
22c. OFFICE SYMBOL	Code 7601

DD FORM 1473, 84 JAN

83 APR EDITION MAY BE USED UNTIL EXHAUSTED
ALL OTHER EDITIONS ARE OBSOLETE

UNCLASSIFIED

SECURITY CLASSIFICATION OF THIS PAGE

INTERIM REPORT NO. 1

METAL GRID BASE HETEROJUNCTION TRANSISTOR OPERATING AT 60 AND 94 GHz

PREPARED FOR

NAVAL OCEAN SYSTEMS CENTER
SAN DIEGO, CA 92152-5000

CONTRACT NO. N66001-86-C-0438
W-4A194

FEBRUARY 1988

HUGHES AIRCRAFT COMPANY
MICROWAVE PRODUCTS DIVISION
3110 WEST LOMITA BOULEVARD
P.O. BOX 2940
TORRANCE, CA 90509-2940

CONTENTS

1.0 INTRODUCTION AND SUMMARY 1
- 1.1 Objective 1
- 1.2 Background 1
- 1.3 Summary 2
- 1.4 Interaction with Other Research Groups 3
- 1.5 References 6

2.0 DEVICE MODELING 7
- 2.1 Analytical Model 7
- 2.2 Plans 13
- 2.3 References 19

3.0 DESIGN AND FABRICATION 21
- 3.1 Design 21
- 3.2 Process Review 23
- 3.3 Base Metal Process 24
- 3.4 Plans 25
- 3.5 References 33

4.0 MATERIALS DEVELOPMENT 34
- 4.1 P-Type Doping of GaAs 34
- 4.2 AlGaAs-COMPOSITION 36
- 4.3 Lateral Epitaxial Growth 37
- 4.5 Hardware Development 38
- 4.6 Plans 38
- 4.7 References ..... 4[illegible]

DTIC COPY INSPECTED

Accession For
NTIS GRA&I ☑
DTIC TAB ☐
Unannounced ☐
Justification

By
Distribution/
Availability Codes
Dist | Avail and/or Special
A-1

FIGURES

2-1 Side view of device configuration used for calculation 16
2-2 Top view of device configuration used for calculation 16
2-3 Circuit model for calculation of expected performance of MGBHT 17
2-4 Series resistances of collector and base 17
2-5 Top view with metal grid 18
2-6 Equivalent circuit for R_B with metal grid 18
3-1 MGBHT device - side views 26
3-2 MGBHT device - top view 27
3-3 Full reticle for MGBHT devices and test patterns 28
3-4 Detail of devices 29
3-5 Summary of process 30
3-6 SEM photograph of a Ti-W stripe before epitaxial overgrowth 31
3-7 SEM micrograph of ~0.4 μm Al lines 32
4-1 SIMS analysis of Zn-doped epitaxial layers 39
4-2 X-ray double crystal diffraction data for an AlGaAs layer on GaAs 40
4-3 "Wheel" pattern used for patterning Ti-W metal 41
4-4 Micrographs of parts of a Ti-W "wheel" pattern on GaAs, with partial epitaxial overgrowth of GaAs, (a) optical microscopy, (b) scanning electron microscopy 42
4-5 SEM photograph of a pad (bottom of picture) together with a pair of Ti-W stripes (upper part of the picture) after epitaxial GaAs deposition. In this run, lateral epitaxy across the stripes was almost complete. 43
4-6 SEM photograph of partial lateral epitaxy of AlGaAs 44
4-7 Lateral width of epitaxial overgrowth of AlGaAs vs. orientation 45

TABLES

1-1 Comparison of PBT, HBT, and MGBHT 5
2-1 Vertical dimensions and doping concentrations for calculation 14
2-2 Horizontal dimensions for calculation 14
2-3 Results of calculation 15

1.0 INTRODUCTION AND SUMMARY

1.1 OBJECTIVE

The objective of this program is to develop a new device structure, the Metal-Gridded Base Heterojunction Transistor (MGBHT), and to realize this device in monolithic amplifier circuits operating at 60 and 94 GHz. The first phase of the program involves developing the materials growth and processing techniques required to demonstrate this device, and building and testing a prototype.

1.2 BACKGROUND

The Metal-Gridded Base Heterojunction Transistor was proposed by H. Kroemer in 1983 [1]. The concept is to reduce the series and contact resistances of the classical Heterojunction Bipolar Transistor (HBT) [2] by incorporating a metal grid, buried within the device, which makes ohmic contact to the base layer. The technology for forming thin metal grids within single crystal GaAs has already been developed for the Permeable Base Transistor (PBT) at the Lincoln Laboratories (see [3] and references contained therein). Thus our approach has been to collaborate closely with Lincoln Laboratories to transfer their technology and incorporate it in the heterojunction device. Simultaneously we are establishing the processes for building heterojunction bipolar devices, mostly by incorporating published techniques.

We have conducted a theoretical analysis, described in this report, to estimate the advantages expected for this particular device design. We find that adding a metal grid improves the base resistance, relative to the HBT, by a factor of about 60 %. Thus while a standard HBT has a value of the maximum frequency of oscillation of about 100 GHz for the geometry that we chose for the calculation, an MGBHT of the same geometry has an f_{max} of 160 GHz. One may

argue that the presence of a metal grid in the MGBHT will allow leakage of emitter current, resulting in reduction of the current gain. But, as will be described in this report, we have a technique to minimize this effect. With this technique, our calculations show that the effect on current gain of the metal grid will be small. Important characteristics and data for the PBT, HBT, and MGBHT are compared in Table 1-1.

1.3 SUMMARY

In addition to the theoretical work mentioned above, we have worked on the device design, process verification, and materials preparation. The prototype design has been established with best estimates of the optimum dimensions. These are based partly on our calculations and partly on reported experience with heterojunction bipolar devices. We have incorporated the Lincoln Laboratories process for preparing W grids, with our own e-beam/optical lithography technique. In the earlier stages, grids of Ti-W were prepared with several-μm widths, and used for extensive experiments with lateral epitaxy by MOCVD. The epitaxial growth has been conducted with both GaAs and AlGaAs, and essentially complete overgrowth has been observed. We believe this is the first time that epitaxial overgrowth has been reported for AlGaAs, over metal patterns. Investigations were conducted into the use of Zn as a dopant for the base layers. But due to concern over diffusion of the Zn, we abandoned this approach and switched to Be doping. This involved a major overhaul of the MOCVD reactor to allow for vent/run operation with the very low growth rates of Be necessary for the 1000 Å layers needed for this project. Many calibration runs have also been conducted for establishing optimum paramaters for growth of thin doped GaAs and AlGaAs layers in a controlled, reproducible fashion.

1.4 INTERACTION WITH OTHER RESEARCH GROUPS

For the purposes of description of our working approach in this project, we now summarize the interaction that we have had to date with other researchers who are active in this field.

1.4.1 Lincoln Laboratories

Principal Contact: R. A. Murphy

Other Contacts: C. A. Bozler, M. A. Hollis, K. B. Nichols, and R. Calawa

Techniques Transferred:

- MOCVD overgrowth method parameters.
- Tests for orientation - dependence of overgrowth; sent "wheel" masks for optical lithographic patterning.
- Process for cleaning W grid patterns before MOCVD deposition.

Visits /Contacts:

- M. J. Tejwani visited Lincoln Labs. 24 Nov 1986.
- Telephone conversations with K. B. Nichols almost weekly in Jan, Feb 1987.

1.4.2 Naval Research Laboratories

Principal Contact: N. Bottka

Other Contact: R. Stillman.

Visits /Contacts:

- M. J. Tejwani visited NRL 25 Nov 1986. Discussed Be doping in MOCVD.
- Telephone conversations monthly to exchange data on Be doping, handling and di-ethyl beryllium flow conditions.

1.4.3 Dept. of Electrical and Computer Engineering, University of California, Santa Barbara

Contact: H. Kroemer

Visits:

- M. J. Tejwani and S. Bar visited UCSB 17 March 1987.

Discussions:

- Physics of the MGBHT device.
- Techniques for numerical modeling of devices. Kroemer recommended against pursuing numerical modeling of the MGBHT at this stage, because a meaningful simulation would have to be very complex; also the exact device parameters and configuration are not yet known. Instead he suggested postponing the modeling until a prototype device has been built and realistic parameters and dimensions are known.

1.4.4 Others

Informal discussions were conducted on the subject of this work with P. M. Asbeck of Rockwell International, H. Grubin of Scientific Research Associates, and L. F. Eastman of Cornell University.

TABLE 1-1

COMPARISON OF PBT, HBT AND MGBHT

	PBT	HBT	MGBHT
Date proposed	1980	1948	1983
Ref. for proposal	4	5	1
Transistor type	unipolar	heterojnct bipolar	heterojnct bipolar
Configuration	n	npn	npn
Control mechanism: parameter which is modulated	potential barrier	junction potential	junction potential
f_{max} calculated (GHz)	>200	100	160
f_{max} reported (GHz)	150	105	-
Ref. for f_{max}	6	7	-

1.5 REFERENCES

1. H. Kroemer, "Heterostructure Bipolar Transistors: What Should We Build?", J. Vac. Sci. Technol., vol. B1, pp. 126-130, 1983.

2. H. Kroemer, "Heterostructure Bipolar Transistors and Integrated Circuits", Proc. IEEE, vol. 70, pp. 13-25, 1982.

3. C. O. Bozler, M. A. Hollis, K. B. Nichols, S. Rabe, A. Vera, and C. L. Chi, "18.5-dB Gain at 18 GHz with a GaAs Permeable Base Transistor", IEEE Electron Device Lett., vol, EDL-6, pp. 456-458, 1985.

4. C. O. Bozler and G. D. Alley, "Fabrication and Numerical Simulation of the Permeable Base Transistor", IEEE Trans. Electron Devices, vol. ED-27, pp. 1128-1141, 1980.

5. W. Shockley, U.S. Patent 2 569 347, 1948.

6. A. Murphy, private communication, and DARPA EHF Joint Contractors Review, NOSC, San Diego, CA 18-19 February, 1987.

7. P. M. Asbeck, private communication, and DARPA EHF Joint Contractors Review, NOSC, San Diego, CA 18-19 February, 1987.

2.0 DEVICE MODELING

It is important to develop models for the MGBHT device to determine the performance expected from it, and what values must be attained for certain device parameters in order to achieve this performance. Also, it is useful to determine the similarities and differences from other relevant devices such as the PBT and the HBT, to facilitate incorporation of technologies that have already been developed for them.

We have developed a one-dimensional analytical model for the MGBHT in this reporting period. This model predicts a maximum operating frequency of 160 GHz, based on reasonable assumptions for the various device parameters. This compares with a predicted f_{max} of 99 GHz for an HBT of the same configuration. More sophisticated 1-D and 2-D models have been developed for the PBT [1,2,3,4] and the HBT [5]. We have reviewed this literature and plan to develop such a model for the MGBHT in the future. We will discuss our plans for this below.

2.1 ANALYTICAL MODEL

Because of the close relationship between the MGBHT and the HBT, we conduct the calculation first for an HBT. We then introduce the metal grid and find directly the expected enhanced performance. We adopt the configuration and dimensions quoted by the Rockwell group [6,7] for convenience in comparing our results with their experimental and calculated results. The configuration is shown as in side view in Figure 2-1 and in plan view in Figure 2-2. The circuit model is shown in Figure 2-3. The components are as follows:

R_B - base resistance

r_E - intrinsic emitter resistance

R_{EE} - external emitter resistance (series)

R_C - external collector resistance

C_{BE} - base-emitter depletion capacitance

C_D - diffusion capacitance

C_{BC} - base-collector depletion capacitance

The vertical dimensions and doping concentrations are listed in Table 2-1 and the areas ot the relevant layers are given in Table 2-2. The power gain cutoff frequency is

$$f_{max} = (f_T/8\pi R_B C_{BC})^{1/2}$$

where f_T is the current gain cutoff frequency.

$$f_T = [2\pi(\tau_E + \tau_{CC} + \tau_B + \tau_C)]^{-1}$$

where τ_E is the emitter charge time - $r_E(C_{BC} + C_{BE})$

τ_{CC} is the collector charge time = $C_{BC}(R_{EE} + R_C)$

τ_B is the base transit time

τ_C is the collector transit time .

Note that $\tau_B + \tau_C = C_D r_E$

2.1.1 Evaluation of Capacitances

The base-emitter capacitance per unit area is given by:

$$\frac{C_{BE}}{A_E} = \left[\frac{q}{2\{(N_{DE}\varepsilon_E)^{-1} + (N_{AB}\varepsilon_B)^{-1}\}\{V_{bi} - V_a\}}\right]^{1/2}$$

Here A_E is the area of the emitter

q is the elementary electric charge

N_D and N_A are donor and acceptor densities

ε is the dielectric constant

V_{bi} is the built-in potential

V_a is the applied potential.

We have evaluated this for an emitter current density J_E of 5×10^4 A/cm^2. This is a reasonable operating value for this device [8,9]. With this, we find the applied voltage is 1.63 V and with the charge densities and geometry of Table 2-1, C_{BE} is 50.5 fF. Using the same approach, we find that C_{BC} is 18.5 fF.

2.1.2 Emitter Resistances

The intrinsic emitter resistance is

$$r_E = kT/qJ_EA_E$$

where k is the Boltzmann constant and T is temperature. We find r_E is 5.2 Ω. The series emitter resistance is

$$R_{EE} = \{\rho_{EE}X_{EE} + \rho_E(X_E - X_{DE}) + \rho_{EC}\}/A_E$$

with ρ_{EE} = resistivity of emitter cap = 6.25×10^{-4} Ω.cm

ρ_E = resistivity of emitter = 8.90×10^{-3} Ω.cm

ρ_{EC} = contact resistivity of emitter contact = 1×10^{-6} Ω.cm^2

X_{EE} = thickness of the emitter cap

X_E = thickness of the emitter

X_{DE} = depletion depth of emitter = 2.1×10^{-6} cm

These values give a calculated value for R_{EE} of 10.7 Ω.

2.1.3 Collector and Base Series Resistances

The collector series resistance is distributed as shown in Figure 2-4.

$$R_C = R_{CC} + R_{Clat} + R_{Cs}$$

where R_{CC} is the collector contact resistance

R_{Clat} is the lateral resistance

R_{Cs} is the resistance across the undepleted part of the collector layer.

Assuming the dimensions given in Table 2-2 and Figure 2-2, and a contact resistivity of 1×10^{-6} Ω.cm, this turns out to be 9.7 Ω.

Similarly, the base series resistance is (see Figure 2-4)

$$R_B = R_{BC} + R_{Blat}$$

where R_{BC} is the base contact resistance

and R_{Blat} is the base lateral resistance

We assume $\rho_{BC} = 1 \times 10^{-6}$ Ω.cm^2 (Rockwell report a value of 1.2×10^{-6} Ω.cm^2 [7]). This yields $R_B = 18.8$ Ω.

2.1.4 Transit Times

The transit time across the base layer is approximately

$$\tau_B = X_B/v_s$$

where v_s is the saturation velocity of electrons (1.5×10^7 cm/s). Then τ_B is 0.7 psec. The collector transit time is [10]

$$\tau_C = X_C/2v_s$$

where X_C is the thichness of the collector layer. Thus τ_C is 0.43 psec.

2.1.5 Charge Times

The emitter charge time is

$$\tau_E = r_E(C_{BC} + C_{BE})$$

which is 0.35 psec. The collector charge time is

$$\tau_{CC} = C_{BC}(R_{EE} + R_C)$$

and is equal to 0.38 psec.

2.1.6 Addition of Metal-Gridded Base

The above calculation is summarized in Table 2-3. These figures are generally similar to those observed for HBT's by several other groups [7,11,12]. Our

calculated result for f_T is 86 GHz, giving f_{max} = 99 GHz. This is close to the figure of 105 GHz observed experimentally by the Rockwell group [6].

One way to improve the high frequency performance of the device is to reduce X_B, the thickness of the base layer. But this will increase R_B, more than offsetting the improvement. In fact it is clear from the equation for f_{max} that a better approach for improvement of the device would be to <u>reduce</u> R_B while keeping X_B constant. The first step towards achieving this is to extend the base pad right up to, or such that it penetrates slightly the AlGaAs base layer. This can be achieved by means of the lateral epitaxy being developed for this program, and is estimated to give an improvement in R_B of about 23 %. The next step is to incorporate a grid of metal, connecting the base pads, as shown in Figure 2-5, with the emitter layer grown epitaxially over the top. For reasons discussed below, we have chosen the grid to consist of W stripes of thickness 500 Å and width 2500 Å, lying 7500 Å apart. As discussed in the section on processing, we propose to form the stripes with ohmic contacts to the base layer, and a thin coating of SiO_2 on top to reduce the amount of emitter current which passes into the metal. This substantially reduces R_B, while increasing C_{BE} by about 22 %.

As an upper limit, the new base resistance can be represented as the network of resistors shown in Figure 2-6.

Here R_{Li} is the resistance of a metal stripe i

R_{LBCi} is the contact resistance of stripe i

R_{LSi} is the bulk distributed resistance to current flowing into line i

R_{BC} is the contact resistance in the previous configuration without a metal grid

R_{lat} is the previously-calculated lateral base resistance

n is the number of stripes

Assuming again a contact resistivity of 1×10^{-6} Ω.cm^2, and 10 stripes, in our previous geometry R_B is 6.8 Ω. This compares with a value of 18.8 Ω, calculated without the metal grid. The new values for the parameters in this improved device are summarized in Table 2-3: the resulting value for f_{max} is 160 GHz. Thus we see that with values of parameters similar to those which have been measured in similar devices, or which are used in calculations of the performance of other devices, the maximum frequency of oscillation is more than adequate to meet the goal of 94 GHz required by this program. Moreover it is 60 % higher than calculated for the same device without a metal-gridded base.

2.1.7 Current Gain and Choice of Grid Dimensions

Current gains measured for HBT's are typically of the order of 20 to 200 [7,8,12]. While the addition of a metal grid will improve the frequency performance of the device, it may reduce the gain by allowing emitter current to flow directly into the metal. As discussed in the section on processing, we plan to minimize this effect by coating the metal stripes with a thin layer of SiO_2. This will have the effect of allowing electrons into the metal only through the edges, where the contact is Schottky and the area is relatively small, or from underneath, in the base layer. This loss will be inhibited when we have an AlGaAs base, with graded Al composition. We estimate that the fraction of emitter current lost in this manner will be of the order of a few percent. This means the current gain will be approximately 50, which is acceptable.

We have made no attempt to calculate these phenomena accurately. Likewise, we have neglected the effect of material defects in the overgrown epitaxial material in this analysis. This is because the identities of the defects and their configuration are completely unknown at this stage, and besides the complexity of these phenomena is such that by far the most efficient approach is to measure their effects rather than attempt to predict them theoretically. This philosophy was strongly supported by H. Kroemer in our conversations with him. Based on these considerations, we judge that the best approach is to make the stripes as narrow as practicable with available technologies, with a period of about a micron. Thus we have chosen 0.25 μm for the stripe widths, since this geometry can be readily achieved by electron beam lithography.

2.2 PLANS

Detailed 1-D and 2-D numerical models analogous to those formulated for the PBT and HBT could be developed, and we plan to do so in the future. However, based on our review of the published models, we judge that a detailed numerical model is not justified at this time because of the uncertainties of many of the device parameters. Examples are the contact resistances for the metal stripes to the base layers, and the influence of defects in the overgrown material on current flow. We therefore will delay the development of the numerical model until later in Phase I of this program, when the device processing is more advanced and more experimental data are available. Meanwhile the model described above will serve to establish the expected performance, and processing goals.

TABLE 2-1

VERTICAL DIMENSIONS AND DOPING CONCENTRATIONS FOR CALCULATION

Symbol	Layer	Thickness (μm)	Material	Dop conc (at/cm^3)
X_{EE}	emitter cap	0.05	n^+ GaAs	10^{19}
X_E	emitter	0.1	n $Al_{0.3}Ga_{0.7}As$	5×10^{17}
X_B	base	0.1	p^+ GaAs	2×10^{20}
X_C	collector	0.4	n GaAs	5×10^{16}
X_{SC}	sub-collector	1.0	n^+ GaAs	3×10^{18}

TABLE 2-2

HORIZONTAL DIMENSIONS FOR CALCULATION

Symbol	Layer	Area (μm^2)
-	base	10
A_E	emitter	10
-	collector	28

TABLE 3

RESULTS OF CALCULATION

Parameter	HBT Result	MGBHT Result
F_T (GHz)	86	80
F_{max} (GHz)	99	160
R_B (Ω)	18.8	6.8
r_E (Ω)	5.2	5.2
R_{EE} (Ω)	10.7	10.7
R_C (Ω)	9.5	9.5
C_{BE} (pF)	50.5	72.5
C_{BC} (pF)	18.5	18.5
τ_E (psec)	0.36	0.47
τ_{CC} (psec)	0.37	0.37
τ_B (psec)	0.7	0.7
τ_C (psec)	0.43	0.43

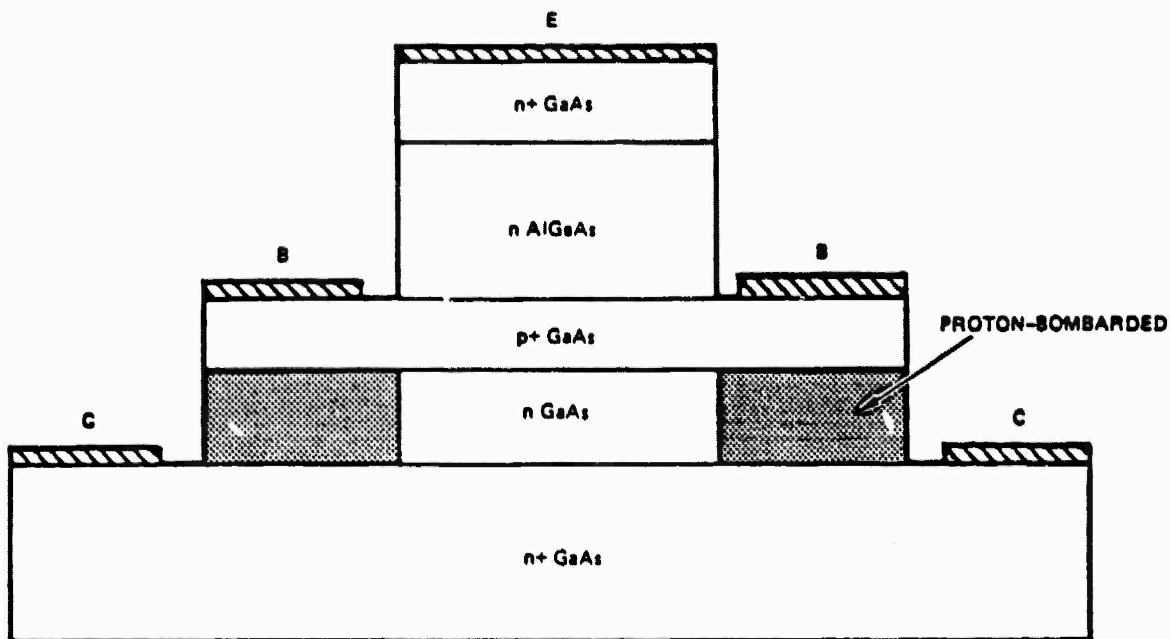

Figure 2-1. Side view of device configuration used for calculation.

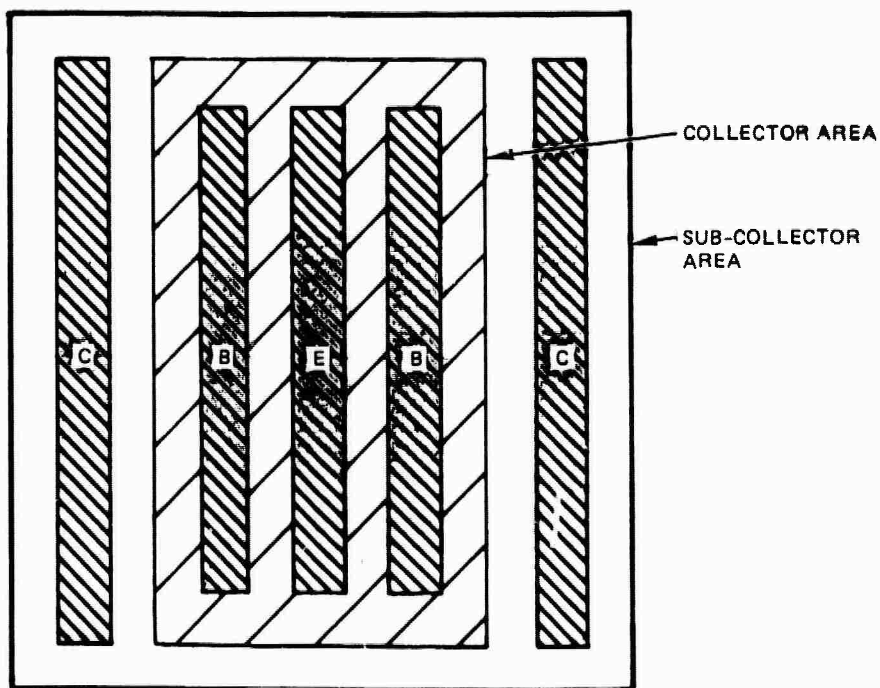

Figure 2-2. Top view of device configuration used for calculation.

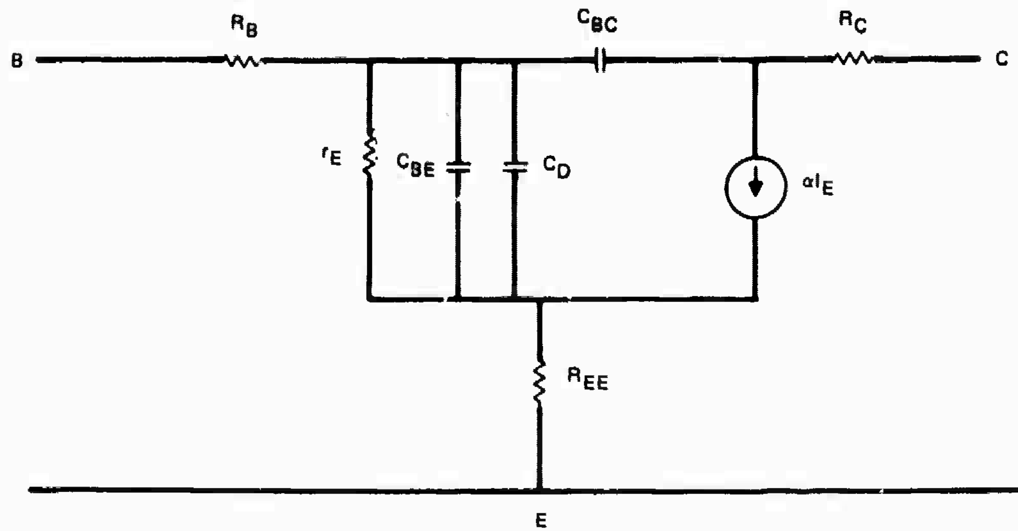

Figure 2-3. Circuit model for calculation of expected performance of MGBHT.

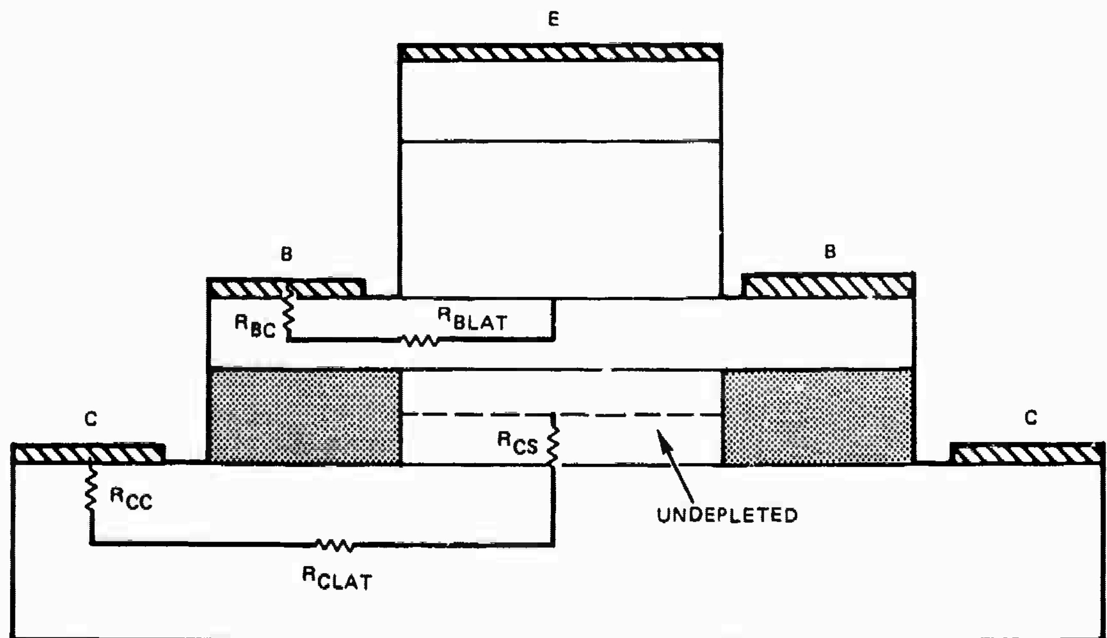

Figure 2-4. Series resistances of collector and base.

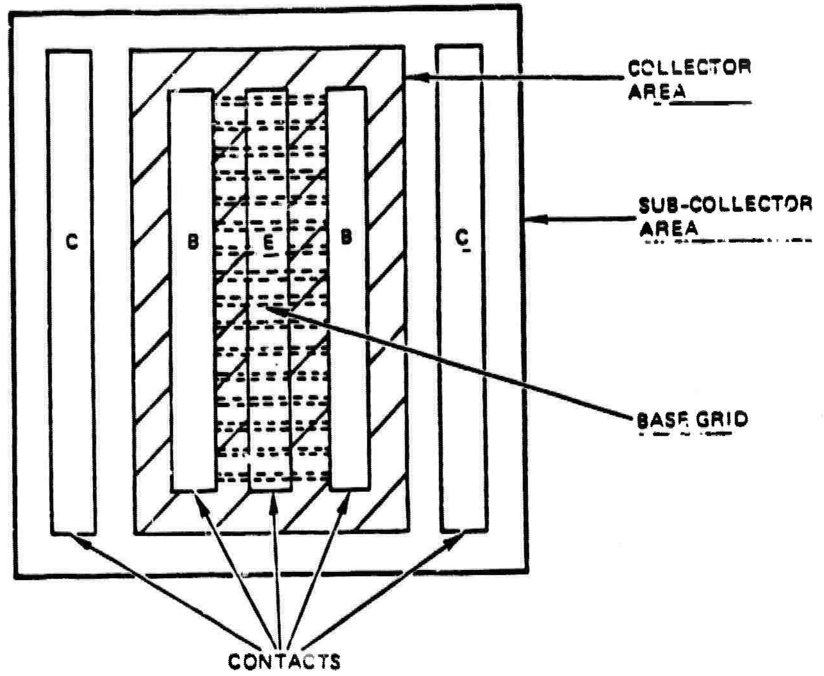

Figure 2-5. Top view with metal grid.

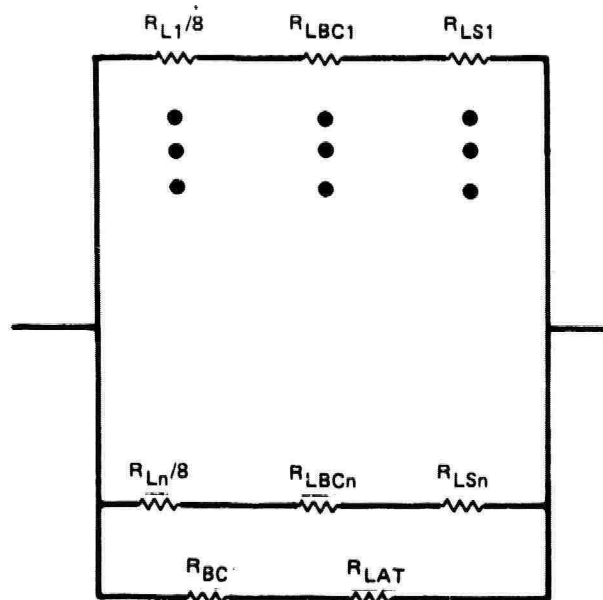

Figure 2-6. Equivalent circuit for R_B with metal grid.

2.3 REFERENCES

1. C. O. Bozler and G. D. Alley, "Fabrication and Numerical Simulation of the Premeable Base Transistor", IEEE Trans. Electron Devices, vol. ED-27, pp. 1128-1141, 1980.

2. G. D. Alley, "High-Voltage Two-Dimensional Simulations of Permeable Base Transistors", IEEE Trans. Electron Devices, vol. ED-30, pp. 52-60, 1983.

3. M. A. Osman, D. H. Navon, T.-W. Tang, and L. Sha, "Improved Design of the Gallium Arsenide Base Transistor", IEEE Trans. Electron Devices, vol. ED-30, pp. 1348-1354, 1983.

4. C.-G. Hwang, D. H. Navon, and T.-W. Tang, "Nonstatic Effects in the GaAs Permeable Base Transistor", IEEE Electron Device Lett. vol. EDL-6, pp.114-116, 1985.

5. P. M. Asbeck, D. L. Miller, R. Asatourian, and C. G, Kirkpatrick, "Numerical Simulation of GaAs/GaAlAs Heterojunction Bipolar Transistors", IEEE Electron Device Lett. vol. EDL-3, pp. 403-406, 1982.

6. P. M. Asbeck, private communication, and DARPA EHF Joint Contractors Review, NOSC, San Diego, CA 18-19 February, 1987.

7. M. F. Chang, P. M. Asbeck, D. L. Miller, and K. C. Wang, "GaAs/(GaAl)As Heterojunction Bipolar Transistors Using a Self-Aligned Substitutional Emitter Process", IEEE Electron Device Lett. vol. EDL-7, pp. 8-10, 1986.

8. H. Ito, T. Ishibashi and T. Sugeta, "High-Frequency Characteristics of AlGaAs/GaAs Heterojunction Bipolar Transistors", IEEE Electron Device Lett. vol. EDL-5, pp. 214-216, 1984.

9. P. M. Asbeck, D. L. Miller, R. A. Milano, J. S. Harris, Jr., G. R. Kaelin, and R. Zucca, "(Ga,Al)As/GaAs Bipolar Transistors for Digital Integrated Circuits, IEDM 1981.

10. H. F. Cooke, "Microwave Transistors: Theory and Design", Proc. IEEE, vol. 59, pp. 1163-1181, 1971.

11. Y. Yamauchi and T. Ishibashi, "Electron Velocity Overshoot in the Collector Depletion Layer of AlGaAs/GaAs HBT's", IEEE Electron Device Lett., vol. EDL-7, pp. 655-657, 1986.

12. M. E. Kim, J. B. Camou, A. K. Oki, K. S. Stolt, and V. M. Mulvey, GaAs IC Symposium, pp. 163-166, 1986.

3.0 DESIGN AND FABRICATION

In this reporting period, the prototype device has been designed, a mask set has been laid out and purchased, and incorporation of the base metal process has been started. In addition, many wafers have been prepared with Ti-W patterns on them for use in overgrowth experiments as described in a later section.

3.1 DESIGN

The prototype device is shown as two side views in Figure 3-1 (a) and (b) and as a plan view in Figure 3-2. The substrate will be semi-insulating GaAs, on which will be grown 1 μm of n^+ GaAs, followed by 0.5 μm of n GaAs. The first layer is the sub-collector, which is doped at 3×10^{18} atoms/cm^3 of Si for purposes of low series resistance, and forming good ohmic contacts. The next layer is the collector which is doped to 5×10^{16} Si/cm^3.

The base will consist of 0.1 μm of GaAs, with p-type doping to a concentration $0.5 - 2.0 \times 10^{20}$ at/cm^3. This thickness was established by a rough trade-off between the need to keep the base narrow in order to minimize the transit time for electrons, and the requirement of reasonable series base resistance (> 20 Ω without the metal grid). A high figure for the doping is necessary to achieve low sheet resistivity in the base layer, and low contact resistivity to the metal stripes. The actual figure that is attainable is controversial. Rockwell claim a doping concentration of 2×10^{20} at/cm^3 [1,2], which is the figure used in our calculation. But the actual electrical activation may be less than this. In Phase II of this program, the base will be formed from AlGaAs, with the Al composition graded so as to establish a field across the base, and further reduce the transit time.

The metal grid will be deposited so as to make ohmic contact to the base semiconductor. It was initially proposed that the grid lie buried within the base layer. But in the interests of minimizing leakage of emitter current into the metal layers, we plan to initially try forming the grid <u>on top</u> of the base. This also has the advantage of avoiding interruption of the growth of the base layer. Tungsten was chosen after a detailed survey by Lincoln Labs. indicated it was the highest-conductivity material which could be deposited and patterned with sufficient precision and cleanliness, and which could withstand the high temperatures (700 - 800°C) of the MOCVD process. The metal will be 300 - 500 Å thick - about the minimum required for sufficient conductivity. The stripes will be ~ 0.25 μm wide, with a period of 1 μm. The choice of these dimensions was discussed in section 2.1.7. If necessary, the top of each stripe will be shielded from the emitter by a 600 Å layer of SiO_2. This step, which has been applied to the PBT [3], is designed in the present context to minimize loss of emitter current to the metal. 600 Å is about the minimum thickness of SiO_2 which can form a continuous film

The emitter will consist of 1000 Å of $Al_xGa_{(1-x)}As$ with x = 0.3. This composition serves to establish the larger bandgap in the emitter for high emitter efficiency, while retaining acceptable doping efficiency (higher Al concentrations lead to poorer efficiency). The doping level in the emitter will be 5×10^{17} Si atoms/cm^3. Finally the emitter cap is 500 Å thick, with doping to 10^{19} atoms/cm^3. This serves to provide minimum series resistance and ohmic contact resistivity.

The lateral dimensions of the prototype MGBHT follow closely the optimum

dimensions currently employed for HBT devices [1,2]. This way we are building on the current experience for the optimum configuration of this type of device. It will also facilitate comparison of our results with those of HBT's, first as a check on our processes, and later as we build the full structure, as an experimental comparison of the two devices.

The complete layout is shown in Figure 3-3. It consists of three different regions, which are separated as three different e-beam scanfields. The top region consists of complete devices with different geometries, and slight variations in their detailed configurations. The different designs are numbered 1 through 7. The middle region contains 7 identical patterns which consist of simply a large grid, with pads at each end. These are for checks of the processes for formation of the grids, and checks on the epitaxial overgrowth. The middle region also contains a test device with large pads for probing. The bottom region of the reticle contains test structures for monitoring contact resistances, as well as other patterns for monitoring various other process steps. Figure 3-4 shows detail of a typical device design.

3.2 PROCESS OVERVIEW

The process is summarized in Figure 3-5. The collector layers will be grown by MOCVD on semi-insulating GaAs, followed by the 1000 Å p^+ base layer.

The wafer will then be removed from the reactor for deposition and patterning of the base pads and metal grid. Deposition of the W will be conducted by RF sputtering. The patterning will then be conducted in two stages: first e-beam alignment marks and the base pads will be patterned in a mask metal by optical

lithography, lift-off, and reactive ion etching (RIE). Then the grid patterns will be defined by e-beam exposure. The W will be patterned by RIE. The metallization and etching steps will based on the processes developed by the Lincoln Laboratories. These have been communicated to us in the frequent contacts outlined in Section 1.

The wafer then returns to the MOCVD reactor for completion of the device structure. This involves deposition of n $Al_{0.3}Ga_{0.7}As$ to form the emitter layer, with lateral epitaxial overgrowth on top of the W grid. This process will be discussed in detail in the next section. The emitter growth will be followed by 1000 Å of GaAs for the emitter cap.

When the layer growth has been completed, devise isolation will be achieved by hydrogen implantation. The polycrystalline GaAs which has deposited on the pads, will be removed by optical masking and wet etching. Metal for contacting the W will then be evaporated so it is self-aligned with the etched regions. Deposi-ion and alloying of ohmic contacts will follow. The processing is completed with formation of the overlay, again with optical lithography.

3.3 BASE METAL PROCESS

For initial development of the techniques for epitaxial overgrowth, it was important to have a large number of wafers with relatively wide metal stripes oriented at various angles relative to the crystal axes. The wide stripes were desirable in order to be able to examine the overgrowth by scanning electron microscopy on one growth front without the view being blocked by the other front. The range of angles was necessary because the growth is dependent on the orientation of the metal lines and observation of this phenomenon is

useful for establishing the quality and reproducibility of the epitaxy. For these purposes we have used the "wheel" pattern masks supplied by Lincoln Laboratories. These patterns have ~ 4 μm lines radiating in spoke-like fashion, two for each one degree arc angle.

In the interests of starting the overgrowth work as early as possible, we used the existing Hughes Ti-W process for preparing these patterns, rather than delaying until we had full incorporated the Lincoln Laboratories process for pure W. Deposition was done by DC magnetron sputtering, and the patterning utilized optical lithography and lift-off of an Al etch mask. The Ti-W was then etched by the reactive ion technique. Figure 3-6 shows a SEM photograph of the edge of one of the resulting lines.

In this reporting period, we have incorporated the Lincoln Laboratories process for pure W base metal, in conjunction with e-beam lithography for patterning the grids. We find that the critical parts of this process are 1) achieving full lift-off of the etch mask; and 2) eliminating all residual contaminants from the patterning process. Figure 3-7 shows a pattern with ~ 0.4 μm Al lines. Here the lift-off was successful, but some dark patches, presumably from a contaminant, are evident near the ends of the stripes. These were readily removed by oxygen plasma cleaning.

3.4 PLANS

We plan to complete the full device structure, as described here, within the next couple of months.

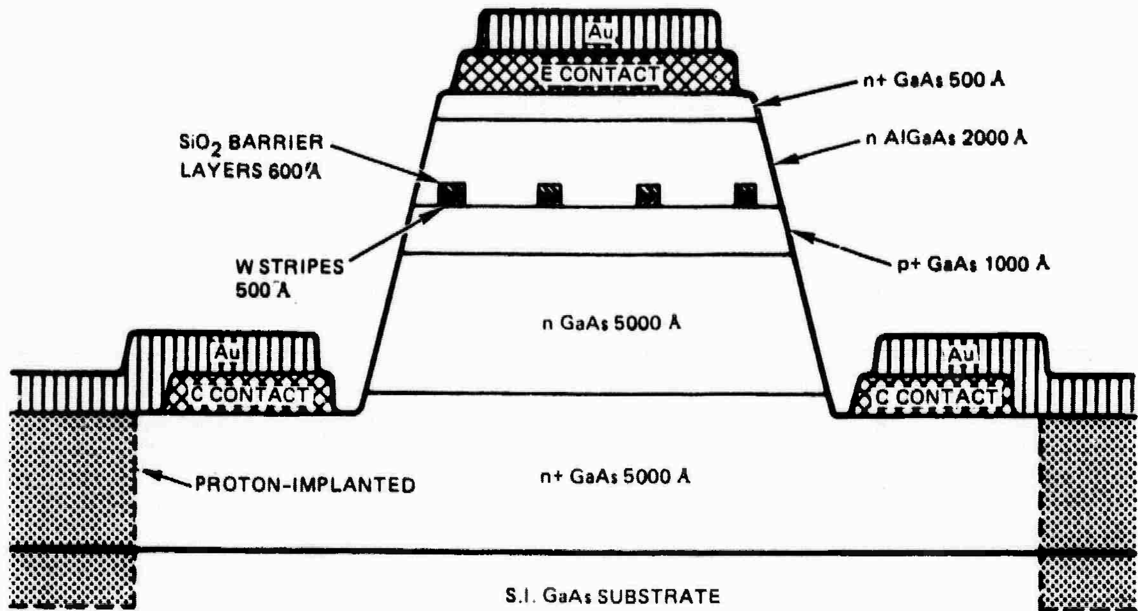

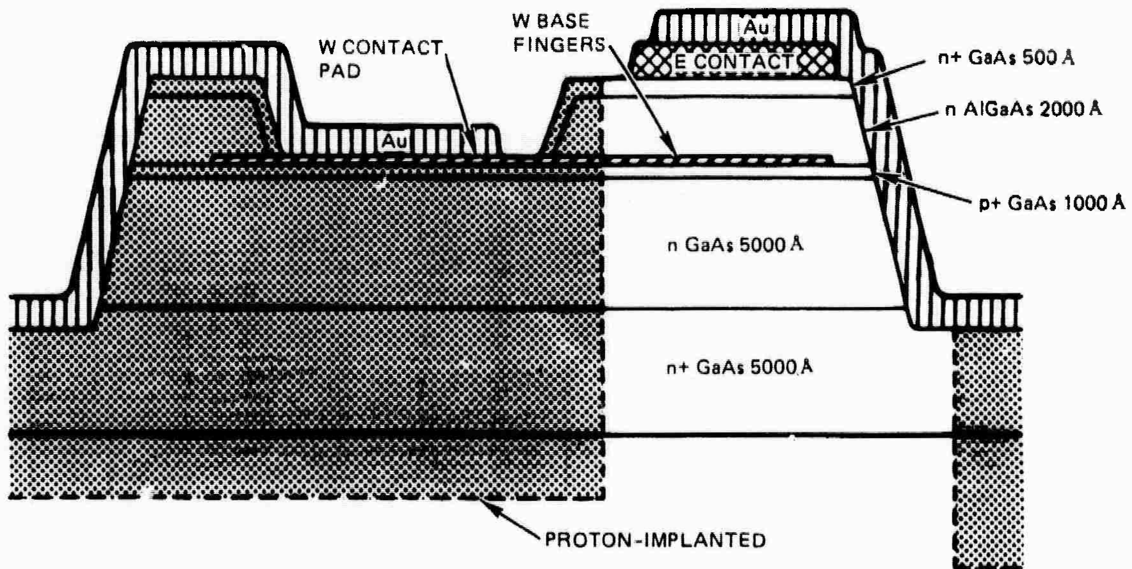

Figure 3-1. MGBHT device - side views.

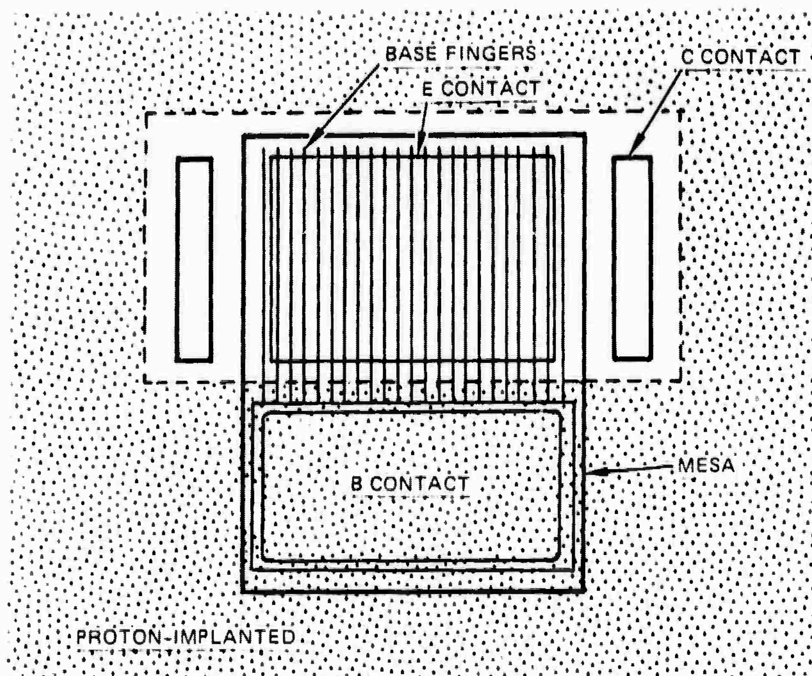

Figure 3-2. MGBHT device - top view.

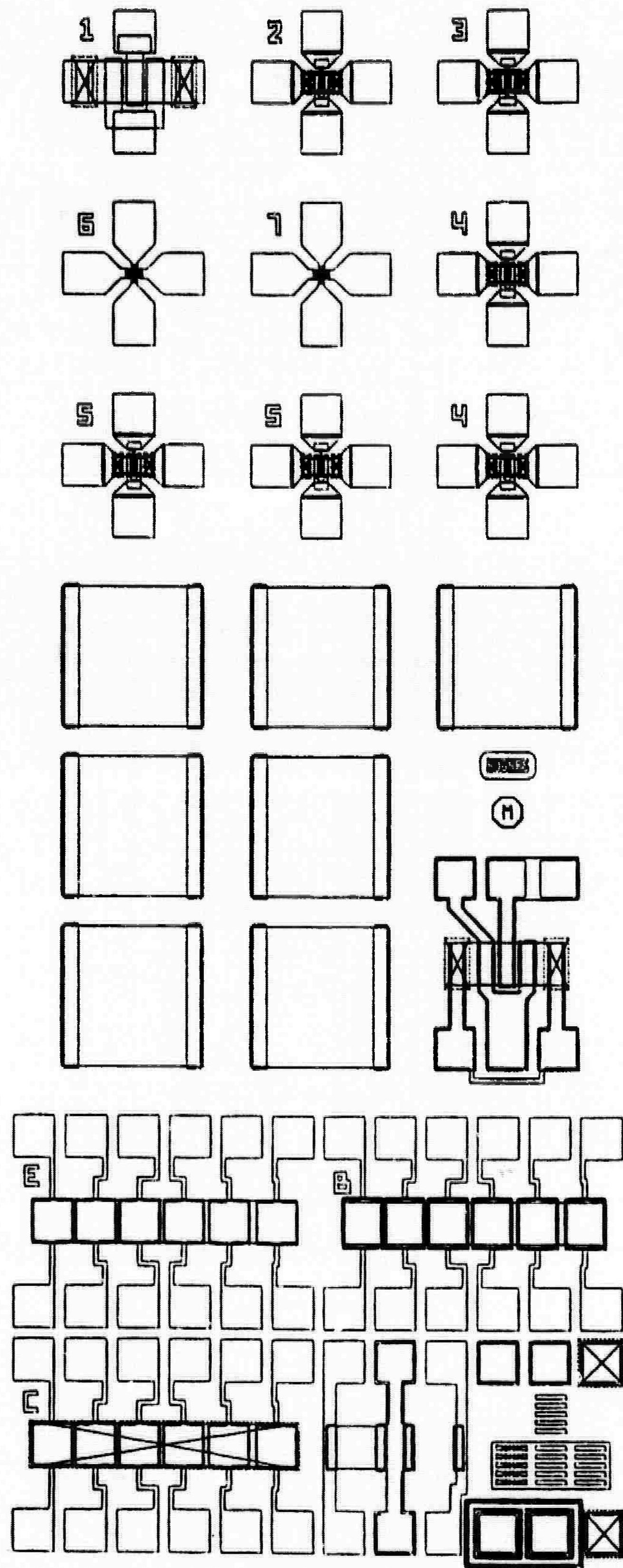

Figure 3-3. Full reticle for MGBHT devices and test patterns.

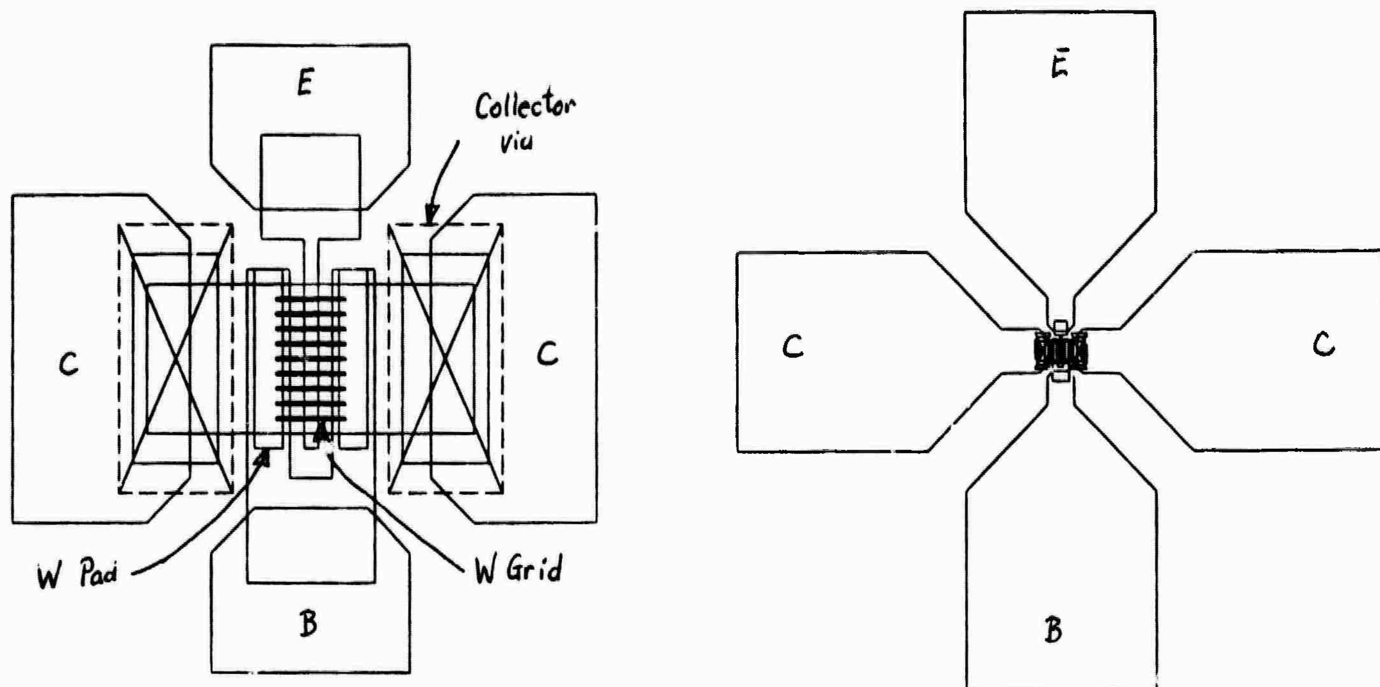

Figure 3-4. Detail of devices.

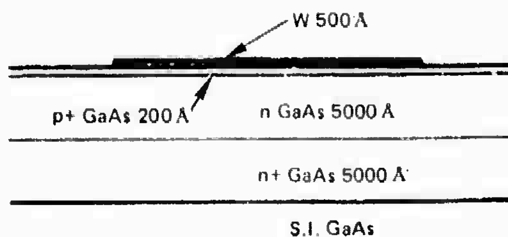

(a) DEPOSIT GATE METAL AND PATTERN

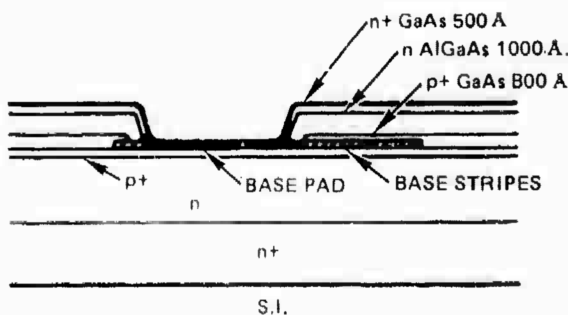

(b) EPITAXIAL OVERGROWTH

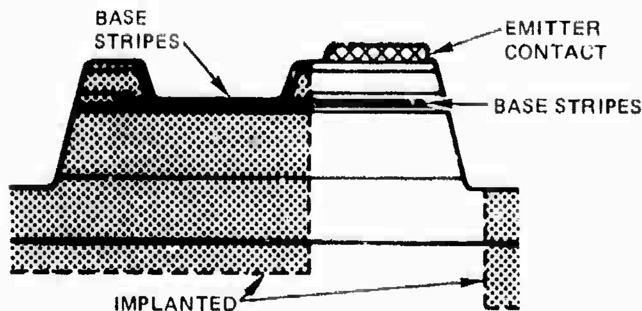

(c) MESA ETCH AND ISOLATION IMPLANTATION

Figure 3-5. Summary of process.

Figure 3-6. SEM photograph of a Ti-W stripe before epitaxial overgrowth.

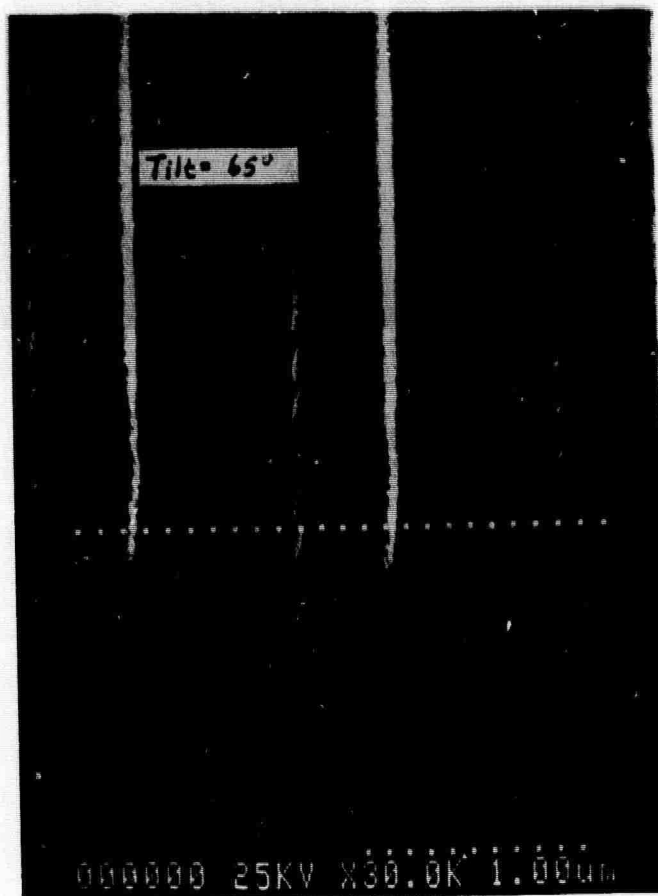

Figure 3-7. SEM micrograph of ~ 0.4 μm Al lines.

3.5 REFERENCES

1. P. M. Asbeck, DARPA EHF Joint Contractors Review, NOSC, San Diego, CA 18-19 February, 1987.

2. M. R. Chang, P. M. Asbeck, D. L. Miller, and K. C. Wang, "GaAs/(GaAl)As Heterojunction Bipolar Transistors Using a Self-Aligned Substitutional Emitter Process", IEEE Electron Device Lett., vol. EDL-7, pp. 8-10, 1986.

3. S. Adachi, S. Ando, H. Asai and N. Susa, "A New Gate Structure Vertical GaAs FET", IEEE Electron Device Lett., vol. EDL-6, pp. 264-266, 1985.

4. W. Shockley, "Research and Investigation of Inverse Epitaxial UHF Power Transistors", Report No. Al-TOR-64-207, Air Force Atomic Laboratory, Wright- Patterson Air Force base, Ohio, September, 1964.

5. G. K. Reeves and H. B. Harrison, "Obtaining the Specific Contact Resistance from Transmission Line Model Measurements", IEEE Electron Device Lett., vol. EDL-3, pp. 111-113, 1982.

4.C MATERIALS DEVELOPMENT

In this reporting period, we have made investigations of the best species to use as the p-type dopant for the base layers of the MGBHT, and begun detailed studies of the optimum growth parameters for preparing $Al_xGa_{(1-x)}As$ with the desired compositions and doping. We have also conducted extensive investigations of lateral epitaxial growth of both GaAs and AlGaAs. Overgrowth of both have been achieved; this is the first time to our knowledge that lateral epitaxy of AlGaAs has been achieved over a metal layer. On the technical side, we have completely rebuilt the MOCVD reactor to allow Be doping, with very slow growth rates and very abrupt interfaces.

4.1 P-TYPE DOPING OF GaAs

The MGBHT device requires a base layer with p-type doping to a concentration of ~ 1 x 10^{20} atoms/cm^3 and thickness ~ 1000 Å. The abruptness of these interfaces between these layers, which we define as the distance over which the doping drops by an order of magnitude, should be ~ 100 Å. The two candidate elements for p-type doping are Zn and Be. Doping with Zn has been demonstrated with carrier concentrations of ~ 10^{20} atoms/cm^3, thicknesses of ~ 1000 Å, and interface abruptnesses of less than several hundred Å [1]. It has also been demonstrated in our laboratory as a viable dopant for MOCVD - grown GaAs with concentrations up to 10^{20} at/cm^3. Therefore we first chose to investigate Zn doping for use in this program.

For this purpose, n-type layers were grown on semi-insulating substrates, followed by Zn-doped layers with concentrations ranging from 1 x 10^{16} to 1 x 10^{20} at/cm^3. These were annealed at 700°C for 15 minutes, which is approximately the heating cycle that the p-type layers must tolerate during

subsequent layer deposition in the MOCVD reactor. Analysis of the profiles of Zn atoms were then conducted by secondary ion mass spectrometry (SIMS). A typical result of these analyses is shown in Figure 4-1. The curves represent the concentration of Zn atoms and are shown for two conditions: as-grown and after annealing. They both show the Zn-doped layer at the surface, beneath which there is the n-type layer of thickness ~ 0.5 μm. The spike at ~ 0.6 μm corresponds to the interface between the epitaxial layers and the substrate; it arises from slight contamination which was intentionally left there for marking purposes. The curve for the as-grown material shows the Zn concentration at the surface is about 8 x 10^{19} atoms/cm^3, and the thickness (defined as the depth at which the concentration drops below 10^{17} at/cm^3) is 860 Å. The abruptness (for concentrations from 10^{17} to 10^{18} at/cm^3) is about 150 Å. Part of this is due to finite switching times for the gas flows in the reactor, which will be reduced by the upgrade in May. Diffusion during the annealing makes the maximum concentration drop to about 8 x 10^{18} at/cm^3 and the thickness increases to 1140 Å, but the abruptness deteriorates only slightly to 230 Å. Since these numbers are not far from the requirements listed above, we believe Zn doping is potentially useful for preparation of the MGBHT device.

Concurrently with these experiments, we investigated the issues involved with use of beryllium as an acceptor dopant. Work at Hughes Research Laboratories has shown that Be doping concentrations up to ~ 10^{20} and interface abruptness less than 300 Å can be achieved by MOCVD with di-ethyl beryllium (DEB) as the dopant source [2]. However DEB is not readily available commercially. American Cyanamid Company, who had made a special production run for the Hughes Research Laboratories work, were identified before the start of this contract

as the probable suppliers, but were unable to provide a sufficient quantity. Another company (Alpha Industries) have this gas available but it was found at Hughes Research Laboratories that this product contains high levels of compensating impurities. Finally, we were informed in December 1986 by N. Bottka, at the Naval Research Laboratories, that Strem Company supplies DEB of sufficient purity, and we placed an order. Meanwhile, safety measures were organized for handling this extremely toxic chemical.

The reactor was completely overhauled for handling Be in August, and the major calibration runs were completed soon aferwards. Characterization is conducted principally by means of "Polaron" capacitance-voltage measurements. Test runs to date have shown Be doping concentrations of up to 2×10^{19} at/cm^3, and layer abruptnesses of the order of 100 Å for a decade change in concentration.

4.2 AlGaAs - COMPOSITION

A series of about 30 runs have been conducted in order to establish the growth conditions necessary for preparing the AlGaAs layers. The required composition is 30 % Al, 70 % Ga. The composition was monitored by means of x-ray double crystal diffractometry. Typical data from one of the samples grown for this program are shown in Figure 4-2. In this figure, the peak marked S corresponds to diffraction from the GaAs substrate and the peaks 0,1,2,3 correspond to diffraction from the epitaxial layer. The separation of the zero order peak from the substrate peak is a direct measure of the composition of the layer. For the sample of Figure 4-2, x was 36 ± 1 %. Compositions in other samples varied from 27 to 47 %; these data are being used to calibrate the growth process.

4.3 LATERAL EPITAXIAL GROWTH

Extensive experiments have been conducted with lateral overgrowth by MOCVD of both GaAs and AlGaAs. Metal stripes were formed for these studies in so-called "wheel" patterns, by optical lithography with masks supplied by Lincoln Laboratories. In these patterns, pairs of ~ 4 μm lines at 1° intervals radiate from a common center like spokes of a wheel (see Figure 4-3). The parameters which were varied were the tri-methyl gallium/arsine ratio, the temperature, and the flow rate. Analysis was conducted by optical and electron microscopy. Detailed studies of MOCVD lateral epitaxial growth of GaAs have been done at Lincoln Laboratories, so we utilized their recommended growth parameters at the beginning of our experiments. However epitaxial overgrowth of AlGaAs is an extremely new technique, which will not necessarily be the same as for GaAs, so it was important to conduct new parametric studies. The extent of the similarity of the overgrowth of the two compounds should become apparent as our studies progress.

Figure 4-4 shows micrographs of a pad plus some lines, after GaAs deposition. Some overgrowth is evident, as well as some prominent agglomerations of GaAs on the pads. These are observed routinely both at Lincoln Laboratories and at N.T.T. [4]. Figure 4-5 shows an experiment where almost complete overgrowth was achieved. Figure 4-6 shows partial overgrowth of AlGaAs over the metal stripes. We monitored the amount of the overgrowth as a function of orientation of the stripes relative to the <$\bar{1}\bar{1}0$> direction. This was done by mounting the sample in the SEM with the center of the stripe pattern on the vertical axis of rotation of the sample holder. The sample was tilted by 65° about a horizontal axis, and then rotated about the vertical axis, with photos being taken at 10° intervals. Some typical results are plotted in Figure 4-7.

A maximum in the amount of overgrowth is evident at a grating angle of about 70°. This corresponds to an angle of 20° from the <$\bar{1}10$> direction, which is not far from the optimum angle (35°) identified by other workers for the lateral epitaxy of pure GaAs layers [3]. The ratio of lateral growth to vertical growth is about unity, which is what was observed for GaAs at Lincoln Laboratories.

4.5 HARDWARE DEVELOPMENT

The major limitation in the early overgrowth experiments was the inability to control flow rates reproducibly in the MOCVD reactor when the rates are very small. These low flow rates are necessary in order to achieve the small layer thicknesses and sharp doping transitions needed for the MGBHT device. The lowest growth rate at which the flow settings were reliable was 300 Å/min, whereas we need rates of 50 - 100 Å/min. In addition to supplying Be dopant, the new reactor hardware allows depositions at these low rates.

4.6 PLANS

In the immediate future we will be concentrating on growth of the actual structures needed for prototype MGBHT devices. These include both the starting structure with the collector and Be - doped base, and the overgrowth and emitter structure once the base pads have been formed.

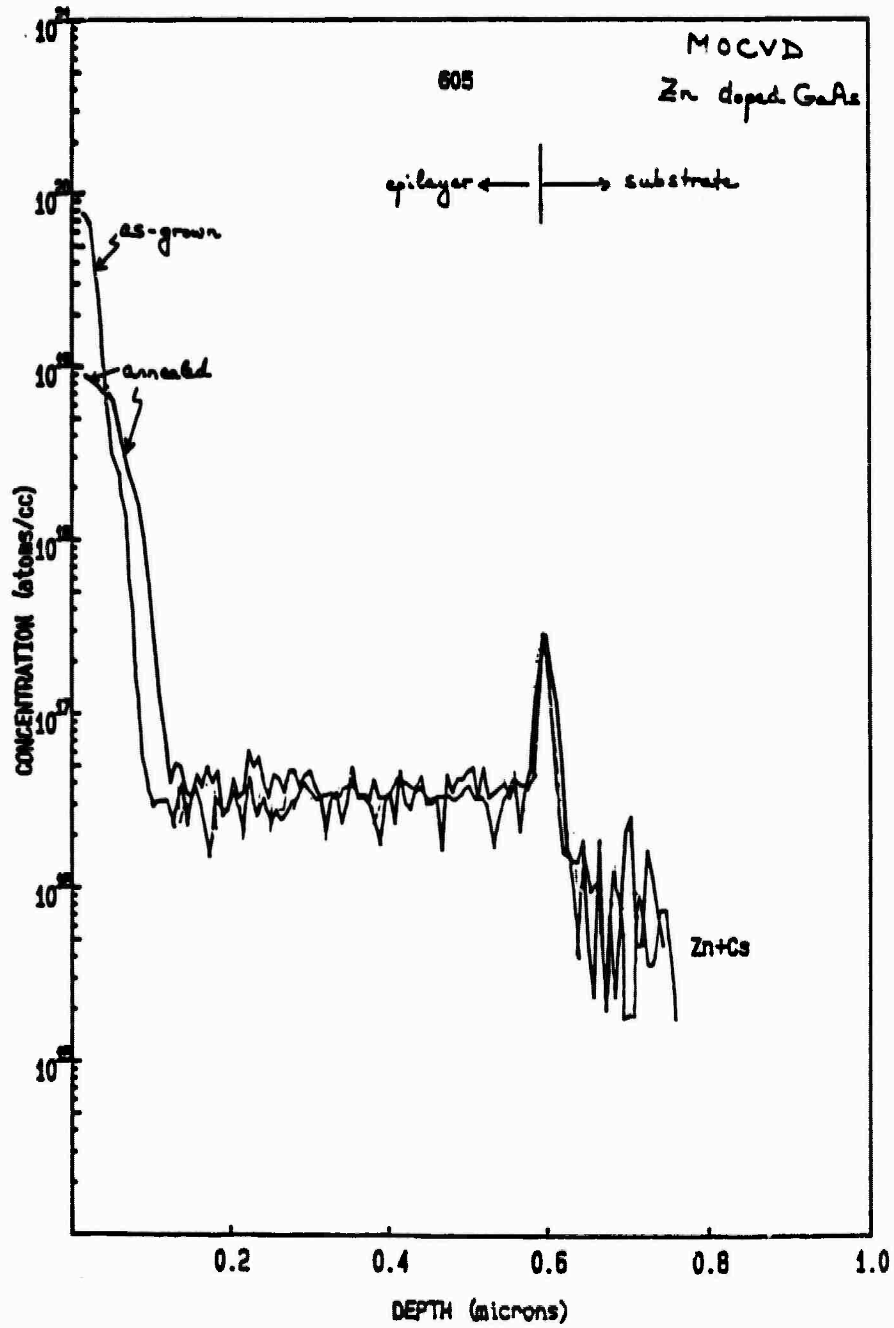

Figure 4-1. SIMS analysis of Zn-doped epitaxial layers.

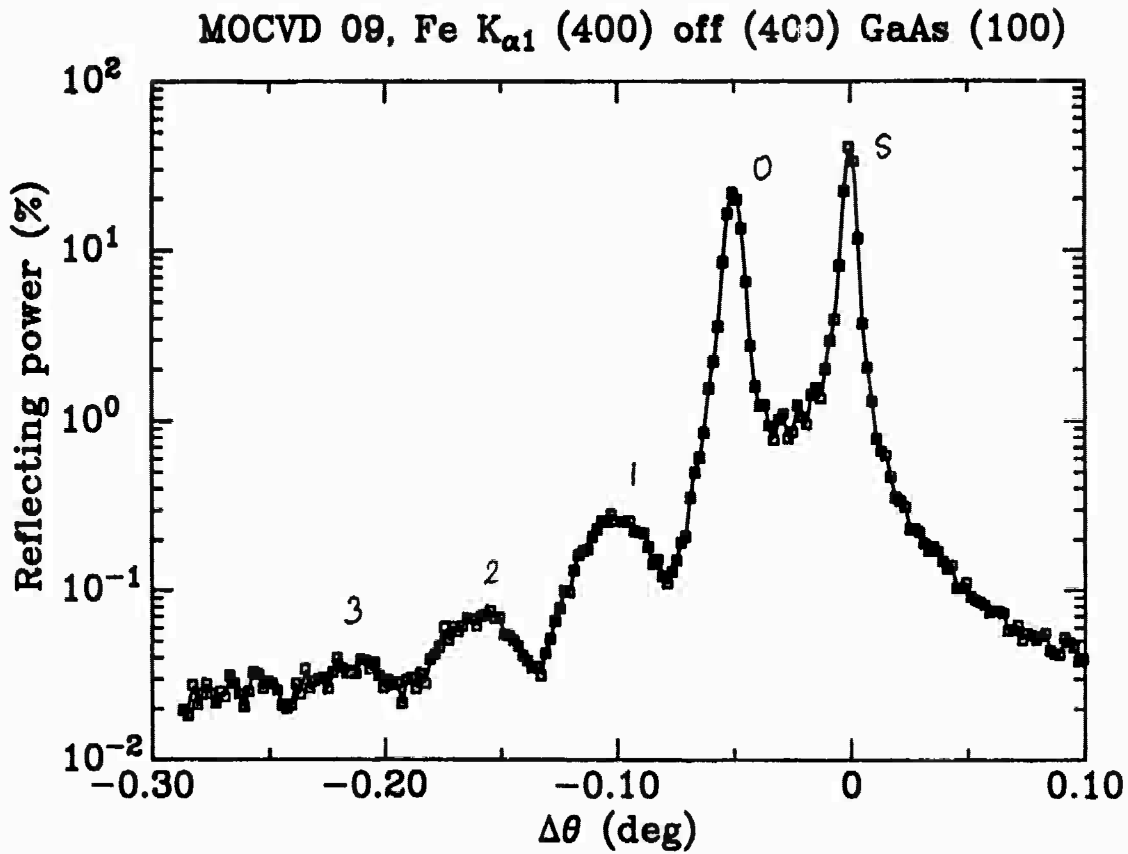

Figure 4-2. X-ray double crystal diffraction data for an AlGaAs layer on GaAs.

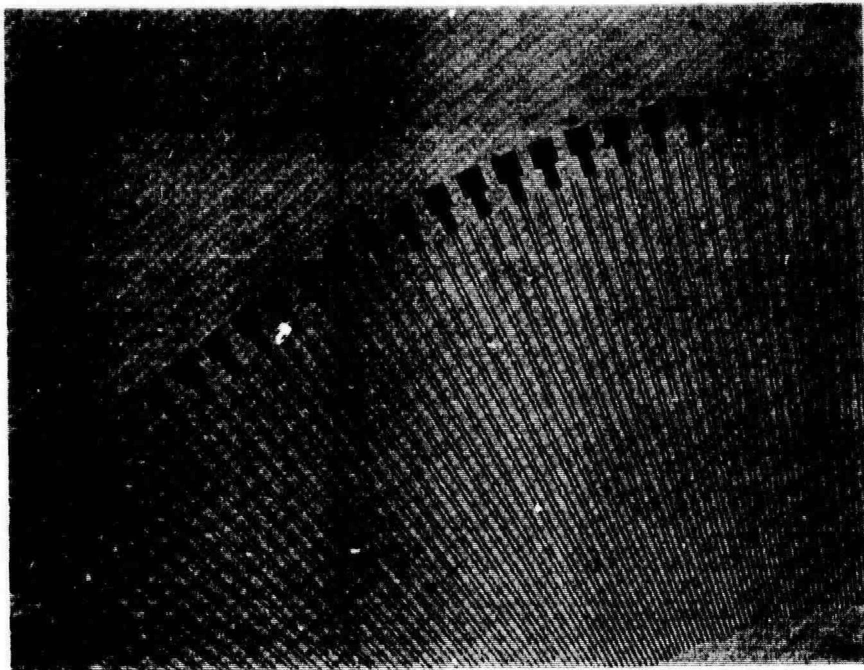

Figure 4-3. "Wheel" pattern used for patterning Ti-W metal.

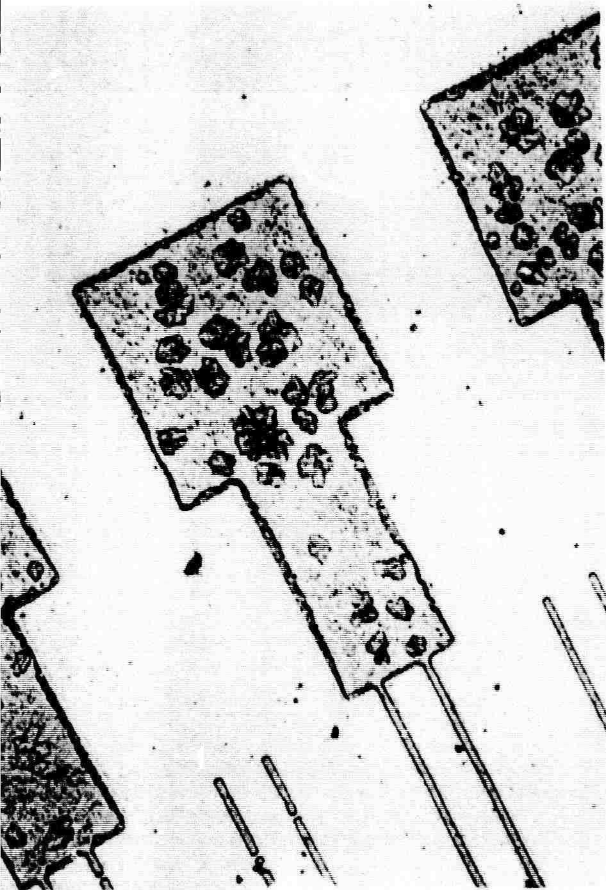

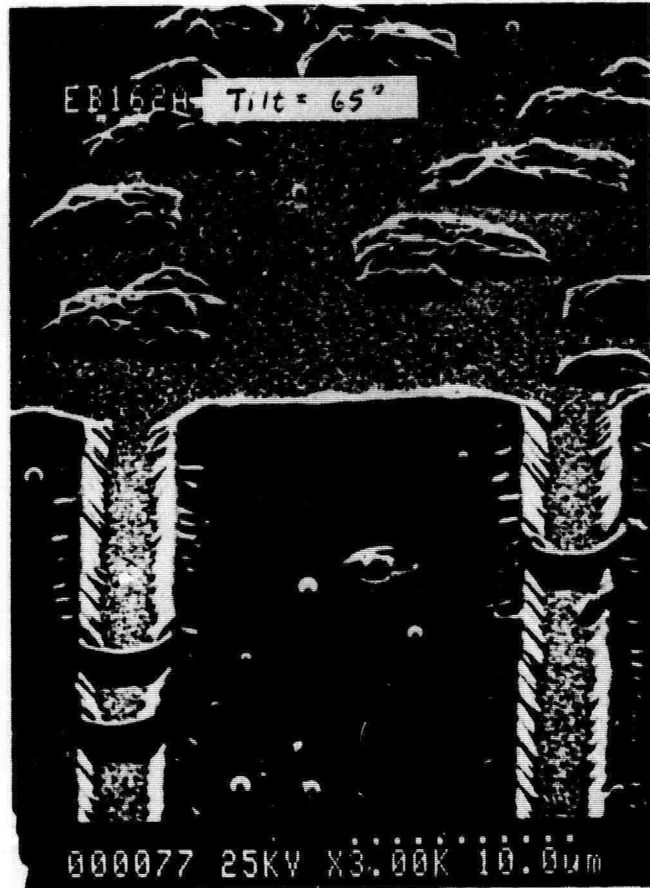

Figure 4-4. Micrographs of parts of a Ti-W "wheel" pattern on GaAs, with partial epitaxial overgrowth of GaAs. (a) optical microscopy, (b) scanning electron microscopy.

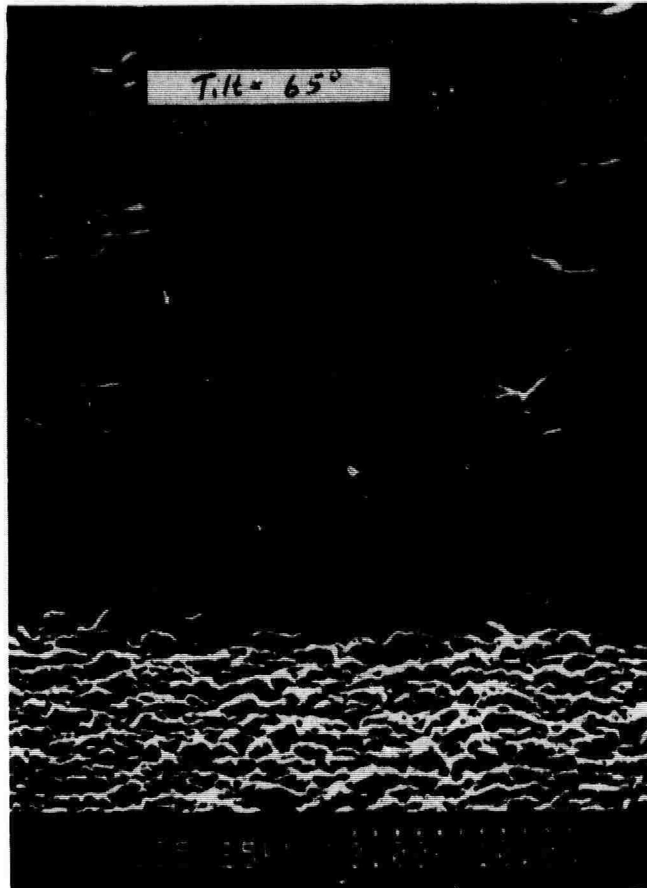

Figure 4-5. SEM photograph of a pad (bottom of picture) together with a pair of Ti-W stripes (upper part of the picture) after epitaxial GaAs deposition. In this run, lateral epitaxy across the stripes was almost complete.

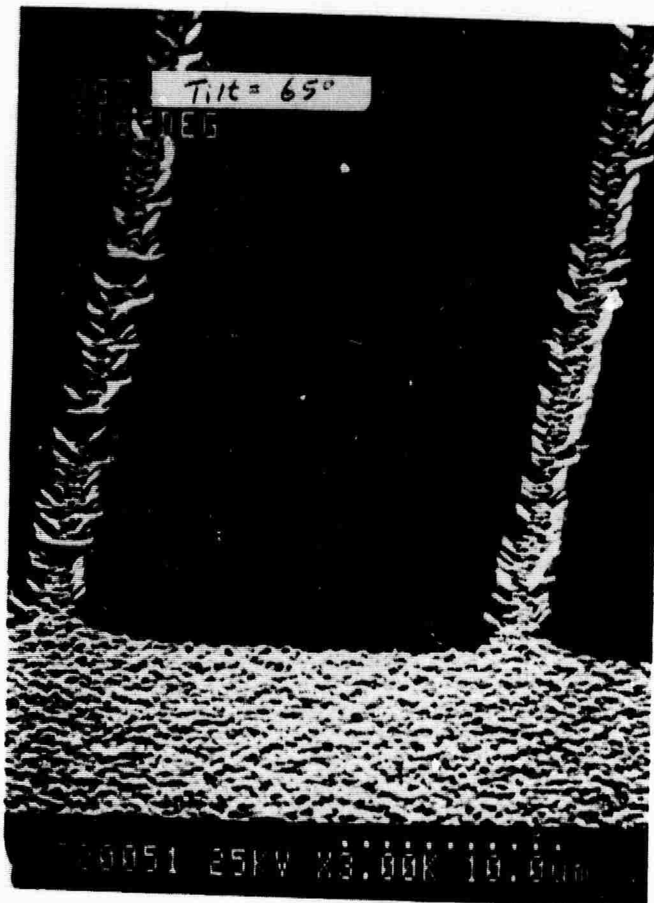

Figure 4-6. SEM photograph of partial lateral epitaxy of AlGaAs.

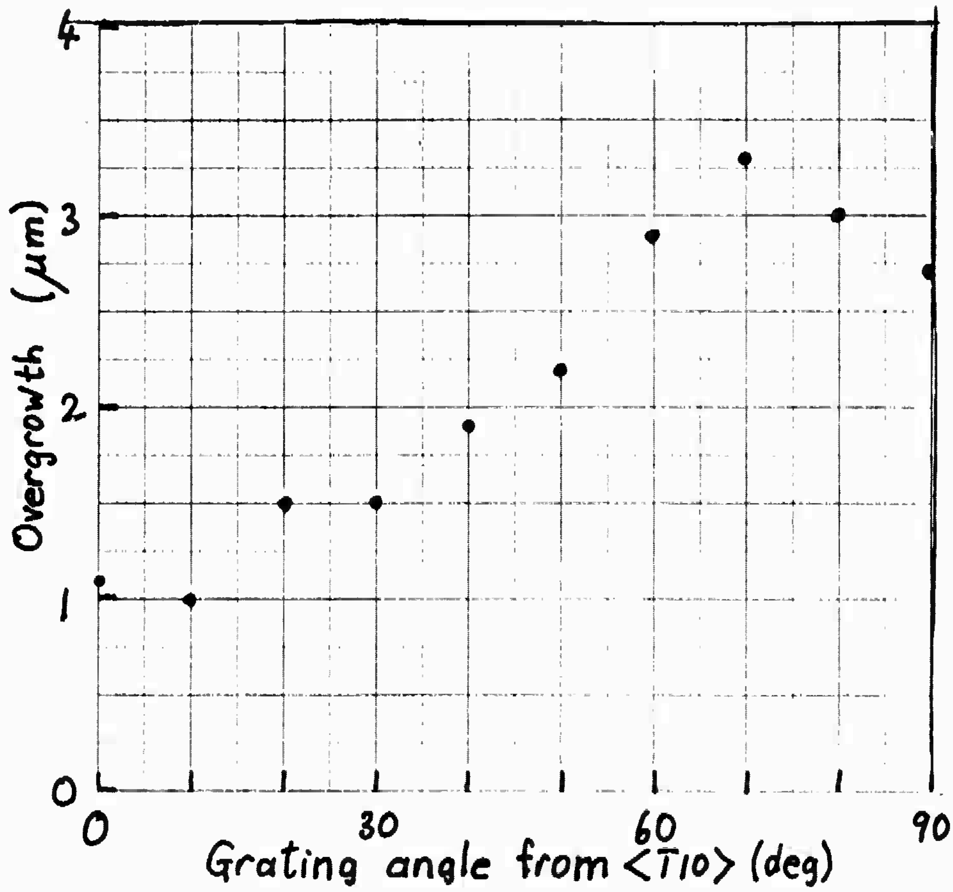

Figure 4-7. Lateral width of epitaxial overgrowth of AlGaAs vs. orientation.

4.7 REFERENCES

1. D. Dobkin and J. F. Gibbons, "Thermal Pulse Diffusion of Zn in GaAs from Elemental Source", J. Electrochem. Soc., vol. 131, pp. 1699-1702, 1984.

2. J. D. Parsons, L. S. Lichtmann, F. G. Krajenbrink and D. W. Brown, "MOVPE Growth of Beryllium-Doped Gallium Arsenide Using Diethylberyllium", J. Cryst. Growth, vol. 77, pp. 32-36, 1986.

3. H. Asai, S. Adachi, S. Ando and K. Oe, "Lateral GaAs Growth over Tungsten Gratings on (001) GaAs Substrates by Metalorganic Chemical Vapor Deposition and Applications to Vertical Field Effect Transistors", J. Appl. Phys., vol. 55, pp. 3868-3870, 1984.

4. S. Adachi, S. Ando, H. Asai, and N. Susa, "A New Gate Structure Vertical-GaAs FET", IEEE Electron Device Lett., vol. EDL-6, pp. 264-266, 1985.